EUROPEAN ORGANIZATION FOR NUCLEAR RESEARCH

CERN-PH-EP/2006-014

8 May 2006

A segmented Hybrid Photon Detector with integrated auto-triggering front-end electronics for a PET scanner

E. Chesi, A. Braem, C. Joram*, S. Mathot, J. Séguinot and P. Weilhammer

CERN, PH Department, CH-1211 Geneva, Switzerland

F. Ciocia, R. De Leo, E. Nappi, I. Vilardi

INFN, Sezione di Bari and University of Bari, Bari, Italy

A. Argentieri, F. Corsi, A. Dragone, D. Pasqua

INFN, Sezione di Bari and Politechnic of Bari, Bari, Italy

Accepted for publication in Nucl. Instr. Meth. A

Abstract

We describe the design, fabrication and test results of a segmented Hybrid Photon Detector with integrated auto-triggering front-end electronics. Both the photodetector and its VLSI readout electronics are custom designed and have been tailored to the requirements of a recently proposed novel geometrical concept of a Positron Emission Tomograph. Emphasis is put on the PET specific features of the device. The detector has been fabricated in the photocathode facility at CERN.

Keywords: Positron Emission Tomography, PET, HPD, front-end electonics
PACS 87.58.Fg; 85.60.Ha; 85.40.-e

* Corresponding author. Christian.Joram@cern.ch

1. Introduction

Hybrid Photon Detectors (HPDs) are advanced photodetectors whose features and properties provide new opportunities for medical imaging. The development discussed in this article is part of an R&D program focused on a novel geometrical concept of a Positron Emission Tomography (PET). It allows for a parallax free 3D reconstruction of the positron source distribution with high spatial and energy resolution over the complete Field of View (FOV).

The *3D axial concept* was proposed[1] as a competitive and innovative approach, mainly for a high resolution brain PET scanner. Sensitivity enhancement is achieved by recovering a fraction of events which underwent Compton scattering in the segmented scintillation detector, leading to a high quality image reconstruction and a reduced scanning time.

We recall first some of the basic principles driving the requirements of the photodetector, in the following called PET-HPD, and the electronic front-end. Section 2 is devoted to a description of the PET-HPD and its components. Section 3 describes the design and properties of the VLSI front-end chip and the data acquisition system. Section 4, finally, summarizes the results of the detector tests.

Our PET concept (see [1-3]) is based on camera modules consisting of axially oriented matrices of 16 × 13 long polished LYSO[2] scintillator bars (e.g. 3.2 × 3.2 × 150 mm^3) optically coupled at both ends to two PET-HPDs (see Fig. 1). The auto-triggering front-end electronics (FEE) is encapsulated in the detector body. A number of camera modules form a complete cylinder around the patient.

The scintillation light produced by a γ interacting in a polished crystal bar propagates by total internal reflection to the ends with an absorption characterized by the bulk attenuation length λ of the crystal and the light path length. The transverse coordinates x and y of the interaction point are derived from the address of the hit crystal. In first approximation and in the absence of cross-talk the resolution is $\sigma_{x,y} = 3.2\ mm / \sqrt{12} \approx 0.9\ mm$. The x-y measurement define accurately the depth of interaction (DOI) and consequently suppress the parallax error when reconstructing the Line of Response (LOR) of a "True" event with two identified back to back 511 keV γ's emitted in the positron annihilation process. The third (axial) coordinate z is derived classically from the ratio of the photoelectron yields N_1, N_2 measured at the two ends of the crystal bar,

$$z = \tfrac{1}{2}(\lambda \cdot ln\ (N_1/N_2) + L), \qquad (L \text{ is the bar length})$$

with an accuracy which depends on the light absorption length λ relative to the length of the bar [1,4]. Moreover, the energy loss in the crystal bar, either by photoelectric effect or by Compton scattering, is determined after correction for the light absorption and calibration from the relation,

$$N_0 = N_1 \cdot e^{z/\lambda} + N_2 \cdot e^{(L-z)/\lambda}\ .$$

The 3D axial PET concept is new compared to standard PETs in clinical operation which are based on radial crystal arrangements in blocks, read out using the Anger logic. It is also different from the *phoswich* [5] approach

---

[1] Patent application filed under PCT/EP02/07967, international publication number WO 2004/008177 A1

[2] The LYSO ($LuYSiO_5$:Ce) scintillation crystal has the following main properties: Photon yield: 32 ph/keV, decay time: 48 ns, peak wavelength: 420 nm, photo fraction at 511 keV: 34.4%.

which also aims to estimate the DOI, however with a coarser resolution and without the possibility of explicitly reconstructing Compton interactions. The concept provides a higher detection efficiency due to the absence of limitations on the radial detector thickness (the γ's can be fully absorbed), and to the possibility to reconstruct unambiguously a fraction (~25%) of γ's which are Compton scattered in the crystal, namely those which are scattered in the forward direction, i.e. when the electron recoil energy is ≥ 50 keV.

A precise measurement of the energy loss in the matrix is important to determine the gamma energy in order to reject scatter events in the organic tissues and, for the discussed concept, to identify the first interaction point in the crystal matrix when a Compton interaction occurs into the forward hemisphere.

The concept consequently imposes very specific constraints on the HPD and the design and performance of the readout electronic concerning sensitivity (detection threshold), dynamic range, resolution in energy and time, as well as counting rate. All these characteristics are addressed when describing the components and the tests of the PET-HPD.

According to simulations [1] and from the tests performed with long crystal bars on the light collection [4], a 511 keV gamma which looses its energy by photoelectric effect in a polished LYSO crystal bar generates photoelectron yields N_1, N_2 of about 500 in each of the HPDs for a standard bi-alkali photocathode response. Assuming a maximum photo detector gain of $5 \cdot 10^3$ (see sect. 4.2) the corresponding charge at the input of the pre-amplifier corresponds to about 400 fC. In order to safely detect a 50 keV recoil electron from Compton interactions, the electronic detection threshold must be ≤ 30 fC. The consequence of operating a PET scanner with such low threshold is a large increase of the counting rate per electronic channel which would result in a high accidental coincidence rate in selecting "True" events. To solve the problem, the HPD and the readout electronic are designed to select two coincident gammas for only those of the events for which the total energy lost in the full scintillator matrix is found within an energy window centred around 511 keV. This is obtained by measuring the induced charge signal on the back plane of the Si sensor (see below) which provides a signal proportional to the total light yield emitted in the matrix.

Following the NEMA-NU2[3] protocol the tests of a brain PET scanner would require an operation with a counting rate of a least 2 MHz/matrix [1], hence more than 20 kHz/channel taking into account the hit multiplicity. Such constraint imposes a time resolution of 5 to 10 ns to the external coincidence logic in order to select "True" events with an acceptable rate of accidentals (Random events).

2. The Hybrid Photon Detector: PET-HPD

HPDs have been chosen for the PET project because of their unique properties for medical imaging applications compared to commercially available standard photon detector (Multi-Anode PMT, Avalanche Photodiodes…). They combine an exceptional spatial and energy resolution with a great flexibility of design (size, geometry). Moreover HPDs of large sensitive area and granularity can easily be tailored as required for the readout of a scintillator matrix.

The charge gain of HPDs is achieved in a single stage dissipation process. The linearity of the response with the incident light is excellent over a large dynamic range and is usually only limited by the performance of the electronics. Moreover the gain is unaffected by variations of the detector temperature.

For photoelectrons (pe's) accelerated up to energies E of typically 15 to 20 keV, the dispersion of the gain (the gain being defined by the number of e-h pairs created per pe in the depleted volume of the Si sensor) is affected by the fluctuation of the energy loss ΔE (straggling) in the inactive entrance layer of the silicon sensor[4], and by

---

[3] NEMA NU2-2001 was proposed as a new standard for performance evaluation of whole body PET scanners. NEMA - National Electrical Manufacturers Association. http://electronics.ihs.com/

[4] The Si sensor is mounted upside down, such that the photoelectrons hit the non-segmented backside.

those (~18%) of pe's which are scattered back from the sensor and deposit only partially their kinetic energy. This last effect is almost independent of the acceleration potential.

The charge gain of the HPD is $g = (E - \Delta E)/w$ with $w = 3.62$ eV per created electron-hole pair and its spread $\sigma_g = [\sigma^2(E/w) + \sigma^2(\Delta E/w)]^{1/2}$, with $\sigma(E/w) = (F \cdot g \cdot N)^{1/2}$ where F is the Fano factor ($F = 0.14$ in Si), and N the number of pe's. The straggling $\sigma(\Delta E/w)$ depends on the acceleration voltage, because of the finite thickness of the inactive entrance layer consisting of a conductive Al layer deposited on the sensor surface for the polarization of the sensor and an ohmic n^+ implant. At high acceleration potential, as will be shown below, the straggling becomes negligible. Experimentally, ignoring the straggling effect at high energies, the measured charge distribution can be characterized by a Gaussian with mean value $\mu = g \cdot N$ and variance $\sigma = g \cdot (ENF \cdot N)^{1/2}$, where ENF is the so called Excess Noise Factor ($ENF = 1.045$ for HPD[5]). Consequently the number of pe's is simply determined by $N = ENF \cdot (\mu/\sigma)^2$.

An important advantage of HPDs for the axial PET concept is, as discussed above, the possibility to read out the induced signal on the Si sensor back plane, providing a fast measurement of the total charge deposited in the depleted Si bulk. This *unique* feature allows for simple and fast photon energy discrimination. To read sequentially all channels and calculate the analogue sum would be much slower and therefore no alternative. Moreover the back plane's fast signals can be used to detect "True" events in coincident detector modules with a time resolution below 10 ns [1].

2.1. The prototype PET-HPD

The prototype PET-HPD developed at CERN [7] is a round[6] proximity focused HPD with a bi-alkali photocathode (QE of about 25% at peak wavelength) deposited on a thin (1.8 mm) flat sapphire entrance window of 105 mm diameter (see Figs. 2 and 3). The total length of the HPD is 67 mm.

The sapphire window, which has excellent mechanical and optical properties (its refractive index is almost matched to the one of the scintillator crystal) is brazed to a metallic ring made of niobium which assures the connection to the photocathode. A set of two electrodes in niobium (0.7 mm thick) inserted in between cylindrical alumina spacers (ceramic) promise a precise 1:1 electron optical image transfer from the photocathode onto the Si sensor.

At the base of the body a skirt in kovar is welded to a stainless steel flange with a sharp knife designed to close the detector at the end of the photocathode processing using a cold indium sealing technique. All the metallic components are joined with the ceramic rings in a single active high temperature brazing step.

The inner lateral surfaces of the ceramic rings receive a special surface treatment[7] in order to control their resistivity and avoid undesirable charging up effect.

On the base plate a ceramic hybrid carrier is mounted which supports the sensor and the readout chips. The control and data connections for the encapsulated ASICs are realized by wire bonding to 40 vacuum feed troughs in the base plate.

Details on the evaporation plant facility at CERN and the photocathode processing can be found in [8].

---

[5] The *ENF* of a HPD is essentially due to the back scattering phenomenon mentioned in section 2. The value $ENF = 1.045$ follows both from an analytical and M.C. calculation.

[6] A rectangular tube with improved active area fraction is foreseen at a later stage of the project.

[7] Photonis-DEP, Brive La Gaillarde, France

2.2. The sensor

The sensor consists of a 300 μm thick rectangular plate of high resistivity silicon (~5 kΩ·cm) produced by SINTEF[8] with 16 x 13 pads implemented as p^+n junctions, DC coupled to the front end electronic. The 208 pads of 3.98 x 3.98 mm^2 with a gap of 40 μm match precisely the crystal matrix configuration. They are arranged in two halves of 8 x 13 pads for the readout, separated by 2 mm. The pad size is larger than the crystal bar cross section (3.2 x 3.2 mm^2) to cope with the light spread on the photocathode due to the finite thickness of the window.

The ohmic n^+ layer implemented on the back side of the sensor (i.e. the entrance window for the accelerated electrons) should be kept thin to minimize the uncollected charge, especially at low electron energies. As will be seen below, in this production run the layer was made about 450 nm thick. In future this can be reduced to less than 100 nm using new equipment now available at SINTEF. The n^+ layer is covered by a 200 nm thick Al film to provide a good electrical contact for the bias voltage. The thicknesses of these layers are important parameters in the interpretation of the variation of the mean collected charge and its dispersion with the acceleration potential (see section 4).

The average load capacity of a pad, including the capacity of the neighbouring pads, routing lines and the capacity to the back plane was measured to be about 5 pF for full depletion ($V_{bias} > 30$ V).

3. The VATA-GP5 chip

3.1. Description

The front end electronics is an integral component of the PET concept consisting of two VATA-GP5 chips of 128 channels each, encapsulated in the HPD body as described above. The chip was designed to be operated in a self triggering mode with a sparse readout option to optimize the data taking rate in a high counting rate environment (up to 2 MHz per HPD).

The VATA-GP5 chip is an optimized version of the VATA-GP3 which was custom developed for the PET-HPD by IDEAS[9] in collaboration with CERN. The prototype we discuss in this paper was produced in standard 0.8 μm N-well CMOS technology. This is adequate for a proof of principle of the PET concept, however in future the chip can be implemented in deep sub-micron technology to optimize the performance in terms of response speed for a full PET scanner.

The chip was designed for use in systems employing several chips in parallel, sharing some control and output lines.

Each channel of the VATA-GP5 features a charge sensitive pre-amplifier/amplifier optimized for a detector capacitance of 5 to 7 pF and input leakage current compensation, automatically and individually adjusted. The pre-amplifier has two programmable gain settings ('LO' and 'HI' which differ by a factor 3), but only the gain 'LO' was used for this project. The total dynamic range extends to 1.2 pC for positive input polarity. The analogue value of a hit channel and the associated channel address can be read out in four different modes: serial (by multiplexing all channels), sparse (by addressing only the hit channels), sparse with adjacent channels and sparse with reading any selection of channels.

---

[8] SINTEF, Forskningsveien 1, P124 Blindern, 0314, Norway

[9] Ideas ASA, Fornebu, Norway

Fig. 4 shows the block diagram of the chip. The analogue chain is a classical arrangement where a Sample and Hold (S/H) signal is applied at the peaking time (adjustable between 200 and 250 ns) of the *slow* shaper when a trigger is detected, in order to store the analogue value for later readout.

In the *fast* chain, the signal from the *fast* shaper of ~40 ns peaking time is applied to a discriminator implemented with a *time walk compensation* circuit to minimize the time jitter of the discriminator for different signal amplitudes. The outputs of the 128 discriminators are OR'ed together and provide the trigger (Fast OR = FOR) for the data acquisition or the possibility to detect coincidences with an expected timing resolution of less than 10 ns.

When a discriminator is activated, the corresponding address of the channel is stored in a register (look up table). In sparse readout mode, if a FOR is detected a veto signal blocks after a minimum time delay (<12 ns) the generation of further ORs, until receipt of a reset signal. Only the analogue values of the hit channels with their address will be read out. This feature is important to reduce the probability of having accidentals recorded when applying the common S/H signal.

Each discriminator can be masked in case of malfunctioning of a channel. There is a common threshold for all the 128 discriminators, but a fine adjustment of each threshold is possible by means of 3-bit DAC. Another feature, not shown in the diagram, is the possibility to inject sequentially into each channel a calibrated charge. Its value is defined by the load of a common external capacitance of 1.8 pF (optionally an internal capacitance is implemented in the chip). This feature is very useful to calibrate the gain of the channels.

While the sparse readout is an essential feature to maximise the data acquisition rate, the serial readout is needed to test the correct functioning of all the channels, to register occasionally the pedestals for subtraction, and to measure the electronic and detector noise.

In sparse mode the data acquisition speed is determined by the readout clock frequency, currently limited to 20 MHz.

3.2. The Data Acquisition system

The data acquisition is performed by a VME interface. A VME slave card, A24 and D32 type, has been built for this purpose. This card generates the three sequences of clocks necessary for the three types of read-out: serial, sparse and sparse with adjacent channels. It contains two pipelined 10 bits ADCs, the first for data in serial and sparse mode, and the second for sparse with adjacents mode.

Software control allows the choice of the read-out mode, together with the control of the masking of channels, the injection of calibration pulses and the setting of the fine tuning of the discriminator thresholds. The format of the data is as follows:

1) Bits 1 → 10: ADC for data in serial and sparse mode.
2) Bits 11 → 20: ADC for data in sparse with adjacent channels mode.
3) Bits 21 → 31: Channel address in sparse and sparse with adjacent channels modes.

The card can read a maximum of 16 VATA chips.

3.3. Tests of the electronic readout chain

3.3.1. Pedestals and amplification gain calibration

The mean value of the pedestals are slightly dependent (within 2 to 4%) on the applied readout mode (serial vs. sparse), and are sensitive to the voltage setting of the power supplies (~5% for 0.1V). Moreover, there is a pedestal shift of few percents if a FOR is generated, in serial and in sparse readout mode, due to some cross-talk inside the chips.

The precise pedestal determination for subsequent online subtraction requires measuring them in the actual readout mode. In sparse mode we injected for each channel four different input charges. The analogue amplitudes

which are measured at the output of the S/H stage are stored in a buffer of the DAQ system. Then, at the end of the sequence, the PC performs a linear square fit (LSF) to the registered data for each of the 256 channels. The extrapolation to zero input charge and the slope of the linear fit per channel provide the pedestal and the gain (per input volt) of the corresponding channel. However, the gain thus determined is only a *relative calibration* of the channels because the absolute value of the injected input charge (the input capacitance is not well determined) is not accurately known. The absolute normalisation of the gains will be determined and discussed in section 4.2 below.

The results of a calibration process are shown in Fig. 5. The mean values of the gain distributions correspond respectively to 198.6 and 184.2 ADC counts per Volt applied to the *calibration* input capacitance. Both chips exhibit a very good uniformity (<1 ADC count or ~0.5%). The difference between the two chips reflects the characteristic dispersion between different wafers. Fig. 6 displays the linearity of the VATA-GP5 amplifier/ shaper response with the injected input charges. Above 1 pC the observed saturation effect is due to the limited dynamic range of the ADC.

Fig. 7 shows the excellent linearity of the discriminator response. The plot has two y-axes. The left one corresponds to the measured charge in ADC counts. For the right axis the calibration of the full electronic chain, which is discussed in section 4.2, has been applied. A threshold of 20 mV - still a safe value avoiding any oscillations - allows detecting signals as low as 30 photoelectrons, corresponding to a 30 keV energy deposition in a LYSO crystal.

The data in Fig. 8, obtained with a threshold of 20 mV, prove that the time walk compensation circuit reduces the slewing time dispersion of the discriminator to less than 10 ns for input charges above 30 fC. This limit corresponds to 50 detected pe's (or ~50 keV deposited energy) if the HPD is operated at 20 kV. Hence the time walk performance matches the PET specific requirements.

3.3.2. Detector noise

Because of the limited range of the ADC (10 bits) used in the interface VME card, a precise determination of the noise was not possible. From the distribution of the pedestals obtained in serial readout mode we derive a fluctuation (σ) of 0.5 to 0.7 ADC counts, hence 0.35 to 0.5 fC corresponding to an equivalent noise charge (ENC) of 2 to 3 thousand electrons.

4. Tests of the prototype PET-HPD

4.1. Experimental set-up

The prototype PET-HPD shown in Fig. 3 was tested using the set-up sketched in Figure 9:. Collimated (~ 5 mm Ø) blue light pulses (~ 470 nm peak wavelength) are generated by a LED (NICHIA-NSPB) which is fired at 50 kHz rate. The duration of the light pulse could be adjusted via the width of the excitation pulse down to a minimum of 10 ns. The pulse duration used for the tests was adjusted to 40 ns. This value is similar to the decay time of the LYSO crystals and, as will be shown below, leads to the number of detected photoelectrons (~500) which one would expect for a 511 keV gamma converting in a LYSO crystal. Exceptionally the duration was increased to larger values to study the response of the slow chain.

The mirror, which reflects the light pulse onto the PET-HPD, could be rotated and translated to permit a scanning of the photocathode surface.

4.2. Experimental results

The set-up allows to scan the light spot over the cathode surface and to establish a mapping between the cathode and the Silicon sensor. This is shown in Fig. 10 for a scan in y-direction. The results in x-direction are fully comparable. The mapping function is well described by a linear function. The observed deviations are of the order of 60 μm (RMS).

Figs. 11 and 12 show Lego plots of the hit and charge distribution of the hit pads for cathode voltages of -10 and -20 kV. At -20 kV the charge on some of the neighbour's pads exceeds the discriminator threshold and consequently increases the hit pads multiplicity however 90% of the light spot intensity is concentrated on two pads (chip 1, addresses 45 and 53). The threshold (~20 fC) eliminates any dark current of the photocathode which would consist of single photoelectrons and leads to background free images.

The total charges measured as the sum of the charges induced on all hit pads above the threshold at -10 and -20 kV are displayed in Fig. 13 including Gaussian fits.

The variation of the mean detected charge μ for the two main hit pads 45 and 53 is plotted in Fig. 14 as a function of the cathode voltage U_C. The Si bias voltage is set at 40 V, well above the value for full depletion. The relation is linear, however it intercepts with the x-axis at U_C = -6 kV due to the relatively thick non-active layer (Al / n^+) at the sensor entrance, which can be improved in a future sensor production. The specific energy loss depends on the initial energy of the electrons[10], i.e. on the cathode voltage. At 20 kV an energy loss ΔE = 1.6 keV is expected. The intrinsic gain of the HPD $g = (E-\Delta E)/w$ at 20 kV is then 5090.

The ratios σ/μ vs. U_C, shown in the same plot for the same two pads, clearly exhibit the straggling effect due to the energy loss in the inactive entrance layer of the Si sensor (see discussion in section 2). The asymptotic values of the ratio (for $U_C \rightarrow \infty$) yield the number of photoelectron according to $\sigma/\mu = (ENF/N)^{1/2}$. We found 507 and 378 for the pads #45 and #53, respectively. From these values and knowing the HPD gain at 20 kV (g = 5090) we calculated the absolute calibration of the electronic chain i.e. the equivalent charge per ADC count. For chip 1 we obtain 0.94 ± 0.01 fC / ADC count, the calibration of chip 2 is about 7.6% lower.

Measurements of the analogue charge output (*slow shaper*) have been performed using a digital oscilloscope. The PET-HPD was operated at 15 kV and the LED was excited with pulses of 5 V ranging from 20 to 250 ns in length. Fig. 15 reveals a perfect linearity of the analogue output signal with the light pulse width. The time delay until the output signal arrives at its peak value scales linearly with the pulse width, demonstrating the remarkable linearity of the integrator over three orders of magnitude. Extrapolation to pulse width zero reveals the intrinsic peaking time of ~220 ns. A shift of the S/H signal of +/- 30 ns with respect to the peaking time changes the measurement of the amplitude by about 2 to 3%. An accurate energy measurement requires consequently a precise adjustment of the S/H signal to the characteristics of the light pulse (i.e. the decay time of the scintillator used).

Finally we measured the relative resolution σ/μ as a function of the length of the light pulse, varying it between 10 and 70 ns. The delay of the S/H signal was not changed. The PET-HPD was operated at 15 kV with an electronic threshold of 30 mV. After quadratic de-convolution of the straggling term discussed above we calculated the number of photoelectrons from $N = ENF\cdot(\mu/\sigma)^2$. The good linearity of N vs. pulse length shown in Fig. 16 underlines the coherence of our approach and demonstrates the level of understanding of the system behaviour.

[10] See e.g. stopping power and energy loss tables provided by NIST http://physics.nist.gov

5. Conclusions

We designed, fabricated and tested a prototype HPD with a set of features and characteristics which are optimized for the readout of a scintillator matrix in a novel PET concept. The 1:1 electron-optical mapping between photocathode and silicon sensor should allow for unambiguous identification of the hit scintillator crystal. The tube can be operated at 20 kV, providing a gain of about 5000. We demonstrated all relevant features of the custom-designed readout chip VATA-GP5. The complete electronic chain was energy-calibrated in an absolute way. The system has an appropriate dynamic range which will allow detecting energy deposits from 30 to well above 511 keV in a LYSO crystal and shows very good linearity. Time walk is efficiently suppressed to better than ±5 ns.

The fabrication of a second PET-HPD tube is under preparation. The next major step in the project is to assemble a complete camera module consisting of a crystal matrix and two HPDs in order to characterize its spatial and energy resolution.

Acknowledgements

We would like to thank our technical staff, F.Cossey C.David, I. McGill and M.van Stenis, (all CERN) for their excellent work in the preparation of the mechanical, optical and electronic detector components.

References

[1] J.Seguinot, A.Braem, E.Chesi, C.Joram, S.Mathot, P.Weilhammer, M.Chamizo Llatas, J.G.Correia, M.Ribeiro da Silva, F.Garibaldi, R. De Leo, E.Nappi, F.Corsi, A.Dragone, F.Schoenahl and H.Zaidi, Novel *Geometrical Concept of a high Performance Brain PET Scanner – Principle, Design and Performances Estimates*, CERN preprint PH-EP/2004-050, accepted for publication in Nuovo Cimento C.

[2] A. Braem, M.Chamizo Llatas, E.Chesi, J.G.Correia, F.Garibaldi, C.Joram,S.Mathot, E.Nappi, M.Ribeiro da Silva, F.Schoenahl, J.Seguinot, P. Weilhammer and H.Zaidi, *Feasibility of a novel design of high resolution parallax free Compton enhanced PET scanner dedicated to brain research*, Phys. Med. Biol. **49** (2004) 2547.

[3] M. Chamizo Llatas, A.Braem, E.Chesi, C.Joram, S.Mathot, J.Seguinot, P. Weilhammer, F.Garibaldi, E.Nappi, F.Schoenahl and H.Zaidi, *High Resolution 3D Brain PET with Hybrid Photon Detector*, Proceedings of 8 th ICATTP Conf. on Astroparticle, Particle, Space Physics, Detectors and Medical Imaging, World Scientific 2004, p. 391.

[4] I.Vilardi, A.Braem, E.Chesi, F.Ciocia, N.Colonna, F.Corsi, F.Cusanno, R. De Leo, A.Dragone, F.Garibaldi, C.Joram, L.Lagamba, S.Marrone, E.Nappi, J.Seguinot, G.Tagliente, A.Valentini, P.Weilhammer, H.Zaidi, *Optimization of the effective light attenuation length of YAP:Ce and LYSO:Ce crystals for a novel geometrical PET concept*, accepted for publication in Nucl. Instr. and Meth. **A**.

[5] W.W. Moses, *Trends in PET imaging*, Nucl. Instr. and Meth. **A** 471 (2001) 209-214.

[6] A.Dragone, F.Corsi, C.Marzocca, P.Losito, D.Pasqua, E.Nappi, R. De Leo, J.Seguinot, A.Braem, E,Chesi, C.Joram, P.Weilhammer, H.Zaidi, *An Event Driven Read-out System for a Novel PET Scanner with Compton Enhanced 3D Gamma Reconstruction*, accepted for publication in IEEE Trans. Nucl. Science, Vol **53,** issue 3 (2006).

[7] A. Braem, E. Chesi, C.Joram, J.Seguinot and P.Weilhammer, *Development of HPDs for Applications in Physics and Medical Imaging*, Proceedings of the Inter. Conf. on New Developments in Photodetection, Beaune (F), 2005, accepted for publication in Nucl. Instr. and Meth. **A**.

[8] A.Braem, C.Joram, F.Piuz, E.Schyns and J.Seguinot, *Technology of photocathode production*, Nucl. Instr. and Meth. **A** 502 (2003) 205.

List of Figures

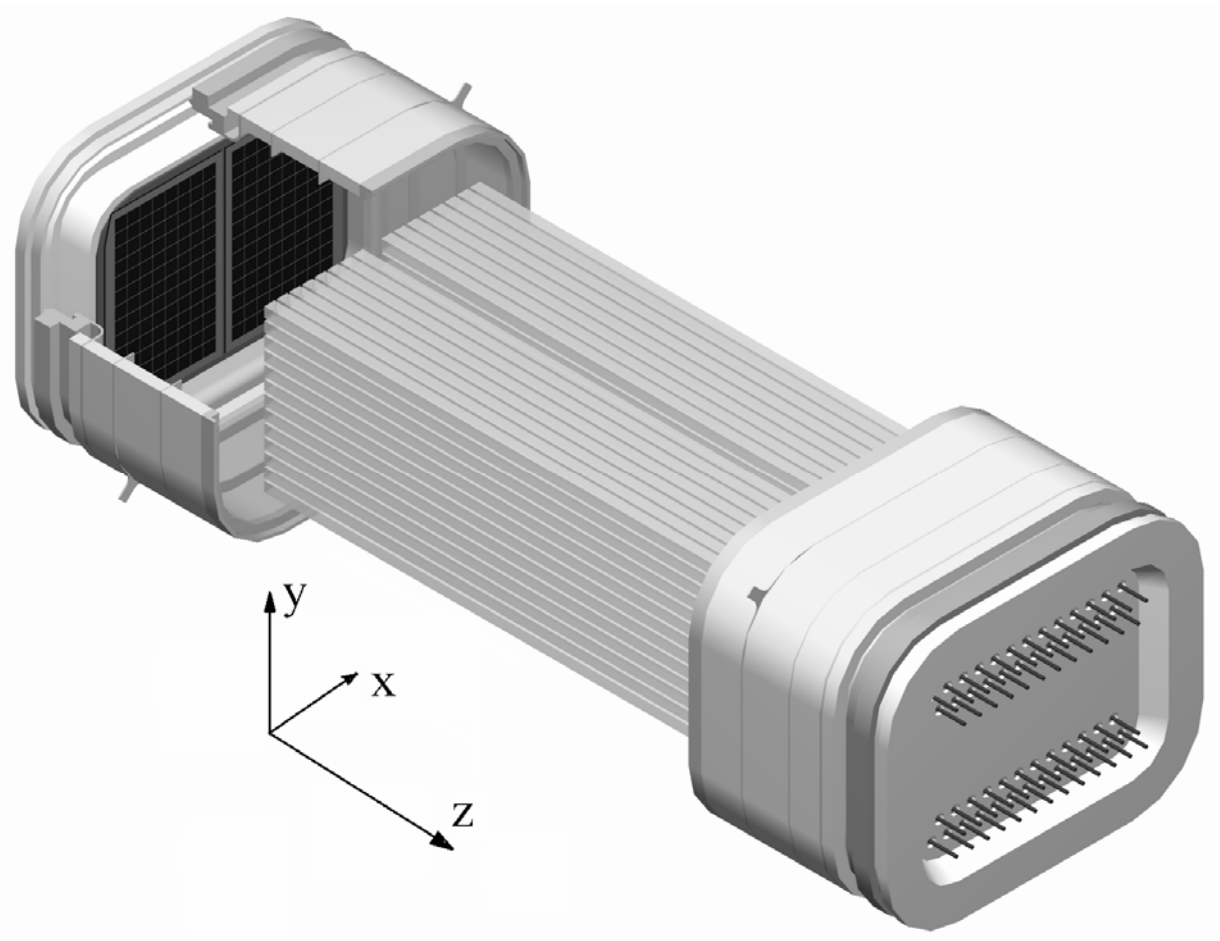

Figure 1: Drawing of a camera module consisting of a matrix of 150 mm long scintillator crystals read out by two (rectangular) HPDs.

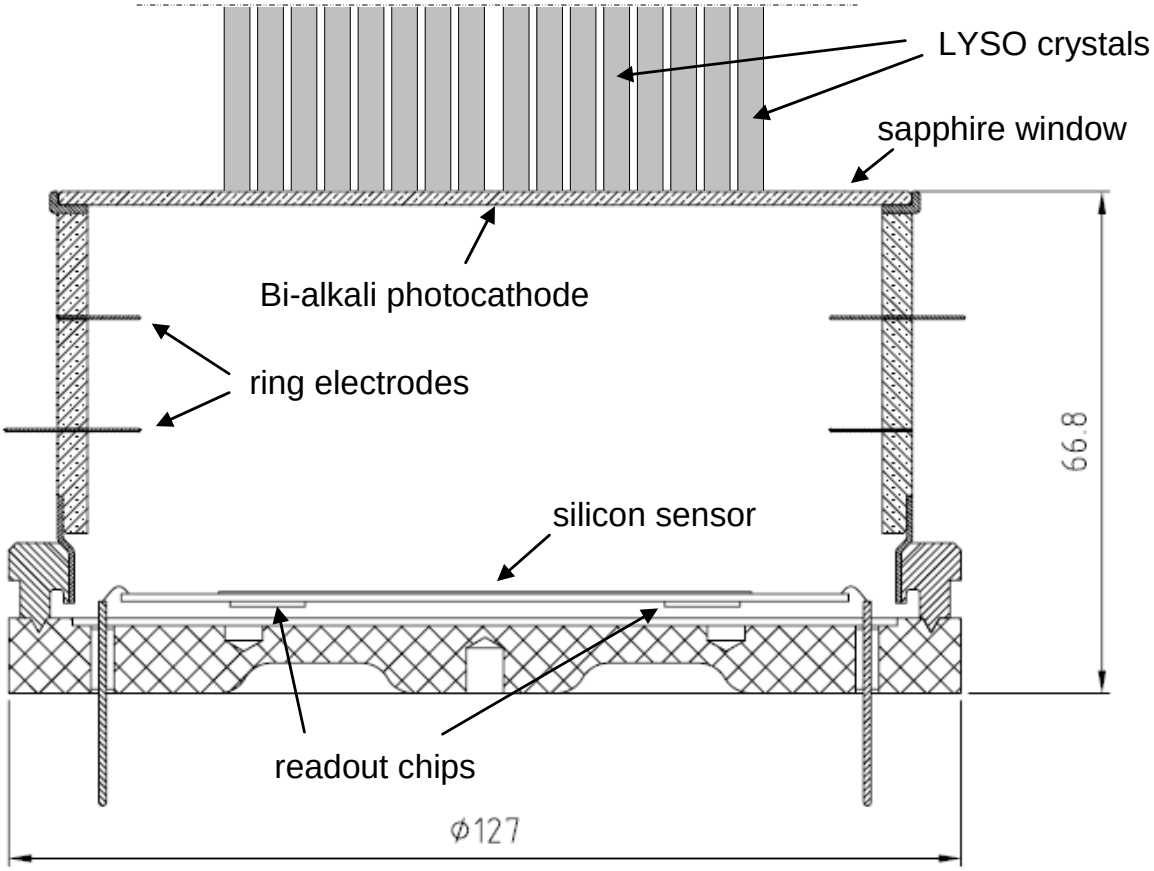

Figure 2: Cross-section of the round PET-HPD prototype with scintillator crystals coupled to it.

Figure 3: Photograph of the sealed PET-HPD prototype tube. The Al-coated Si sensor is clearly visible.

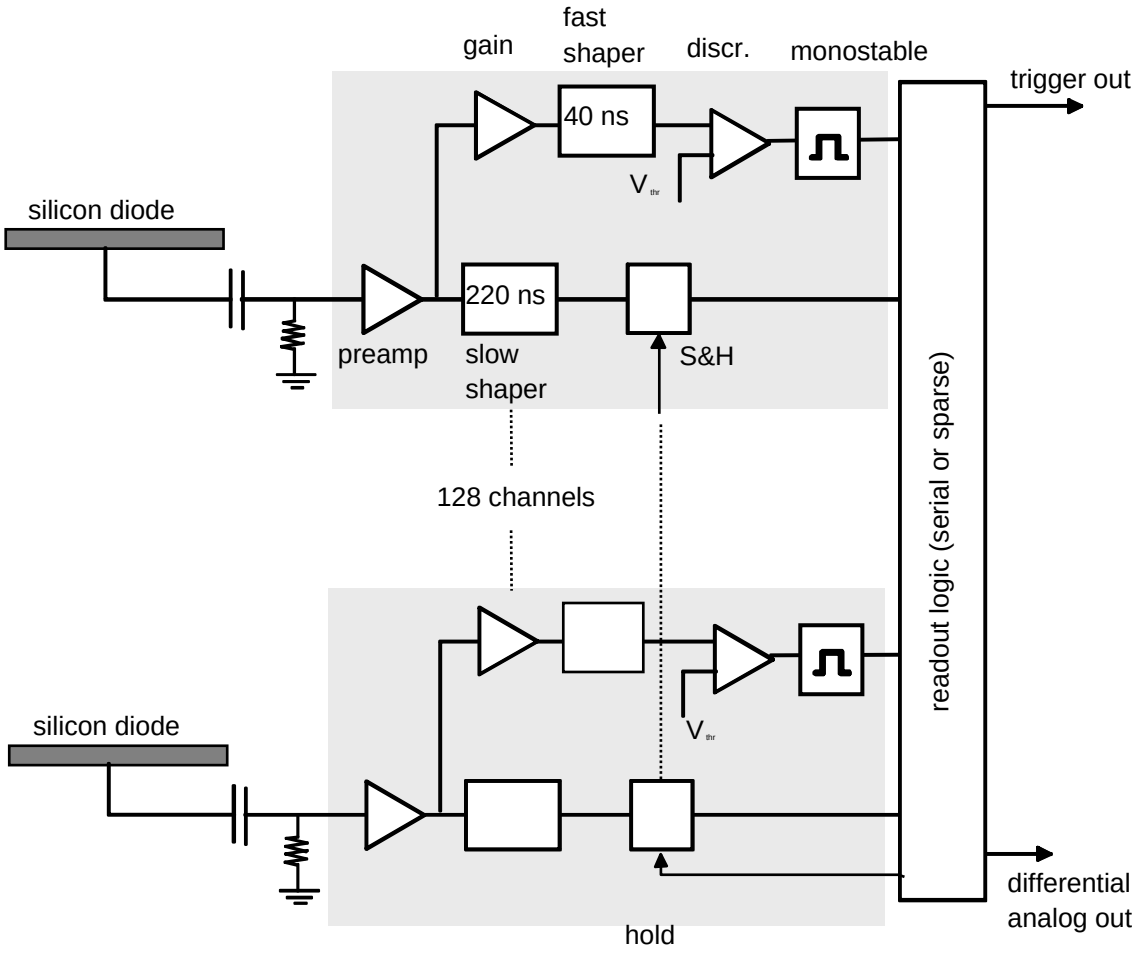

Figure 4: Block diagram of the front-end readout electronic VATA-GP5

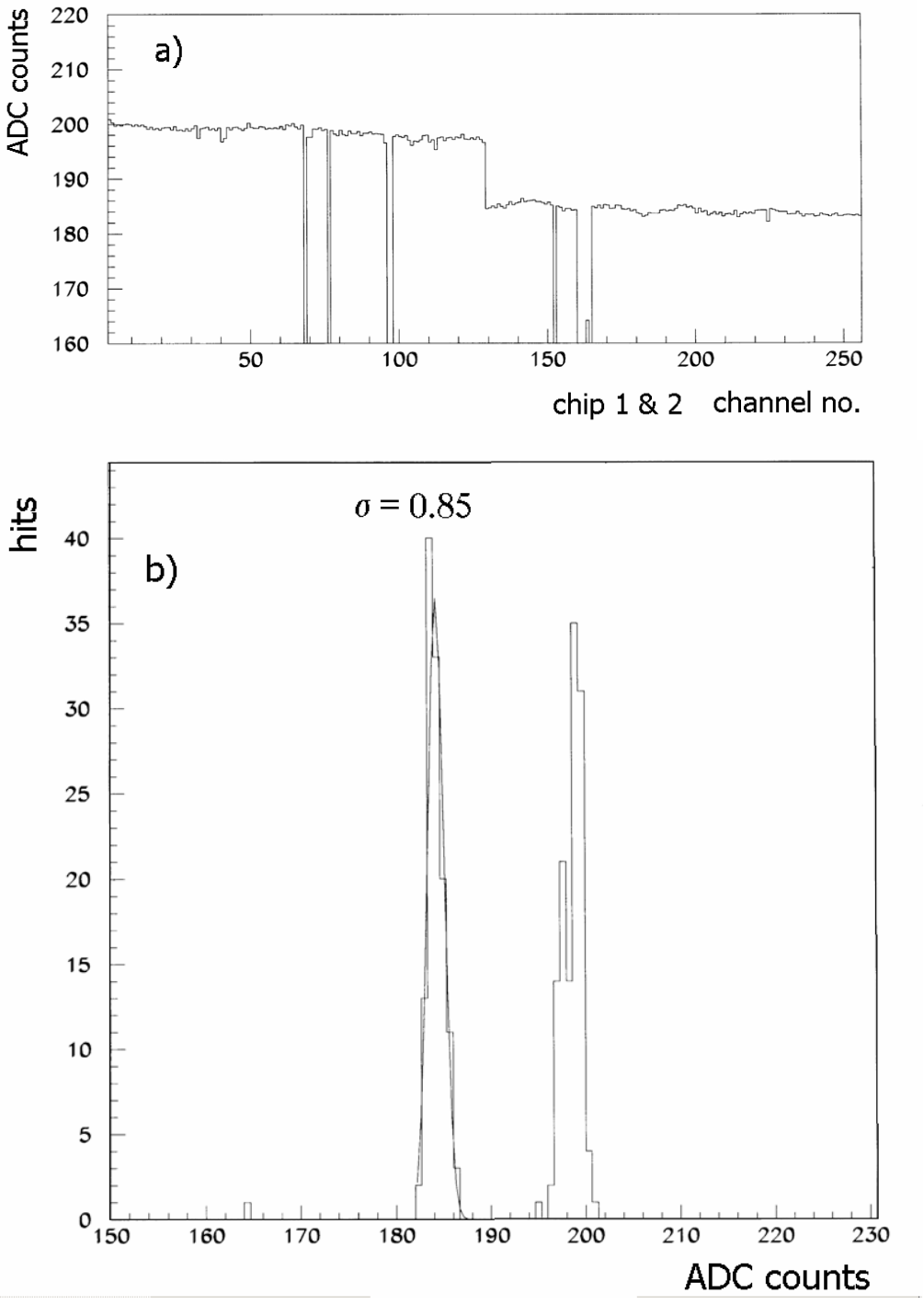

Figure 5: a) Gain distribution of all channels in chips 1 and 2. A few channels are not responding to the excitation pulses however they work under normal operational conditions. b) Histogram of the gains of chips 1 and 2. The gain spread is below 1 ADC count.

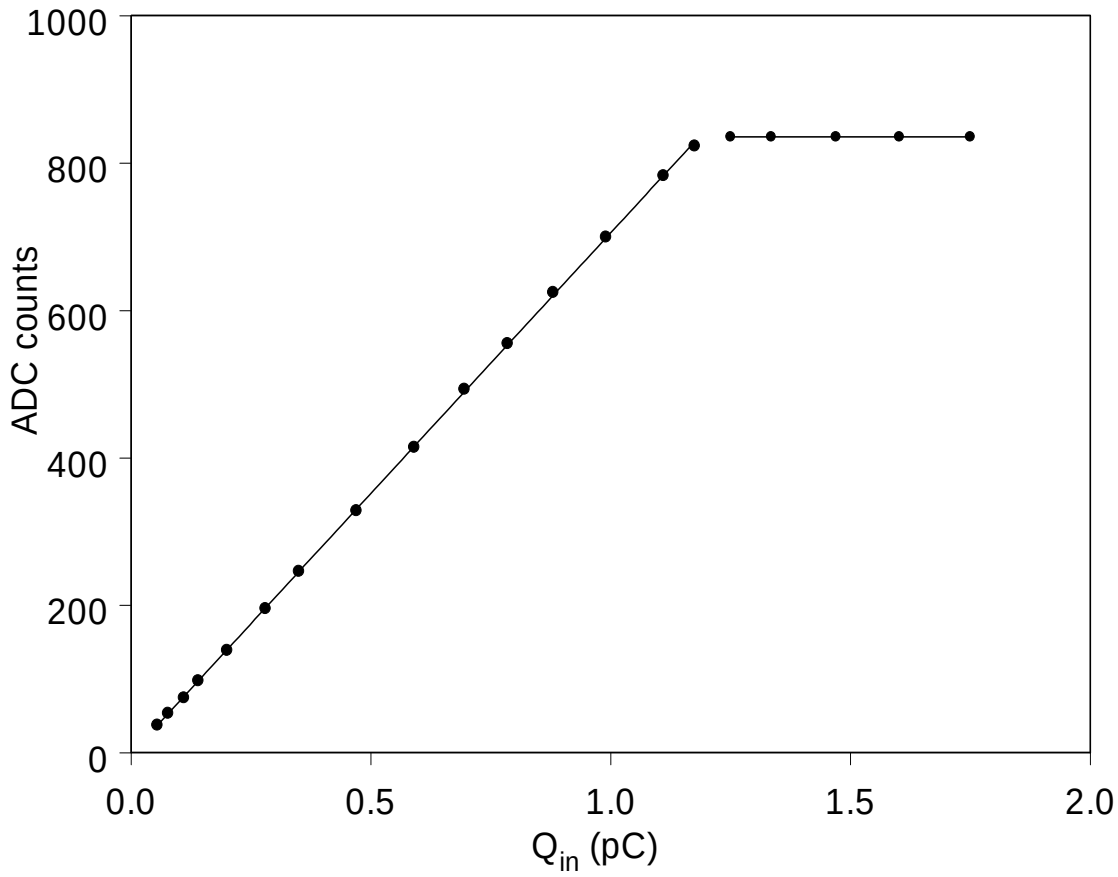

Figure 6: Charge response (in ADC counts) versus input charge Q_{in}

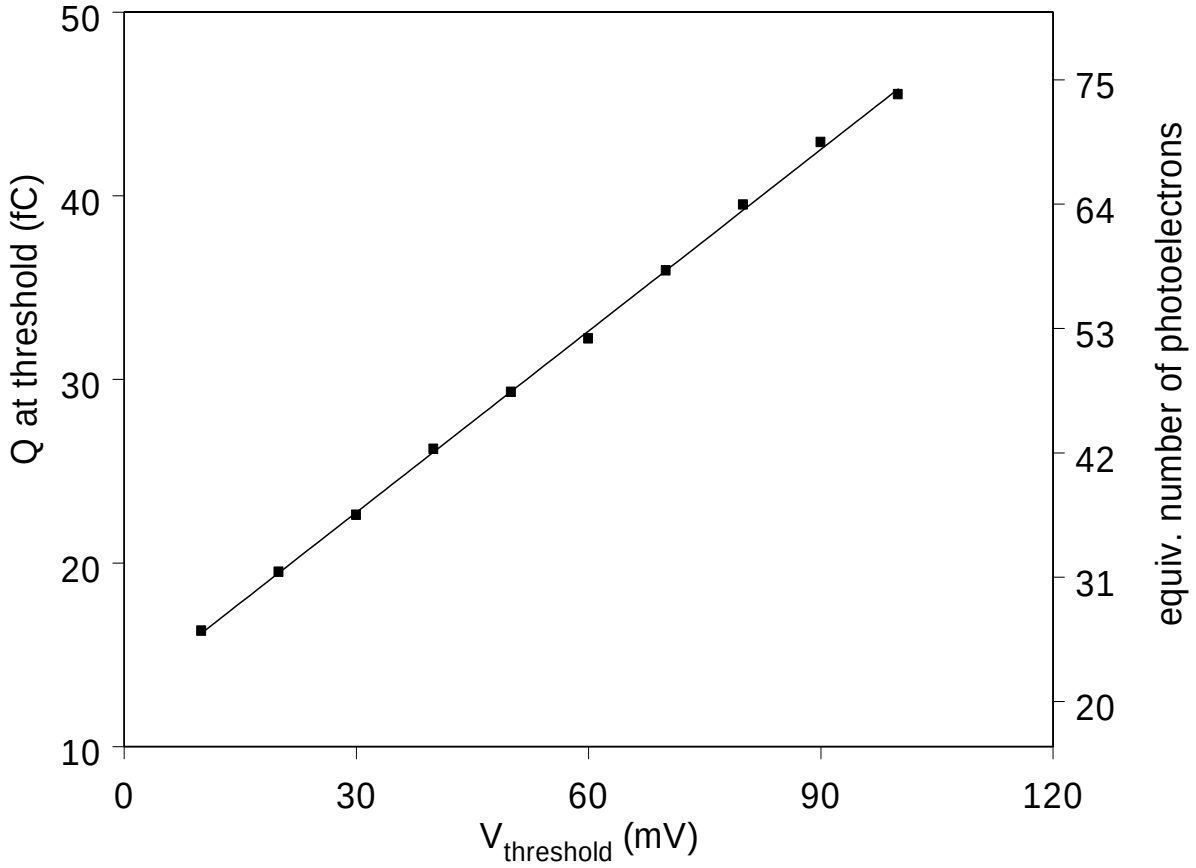

Figure 7: Characteristics of the discriminator. Input charge Q_{in} (ADC counts) versus threshold voltage U_{th} (mV). The preamplifier is operated with gain 'LO'. N_{pe} at threshold versus U_{th}.

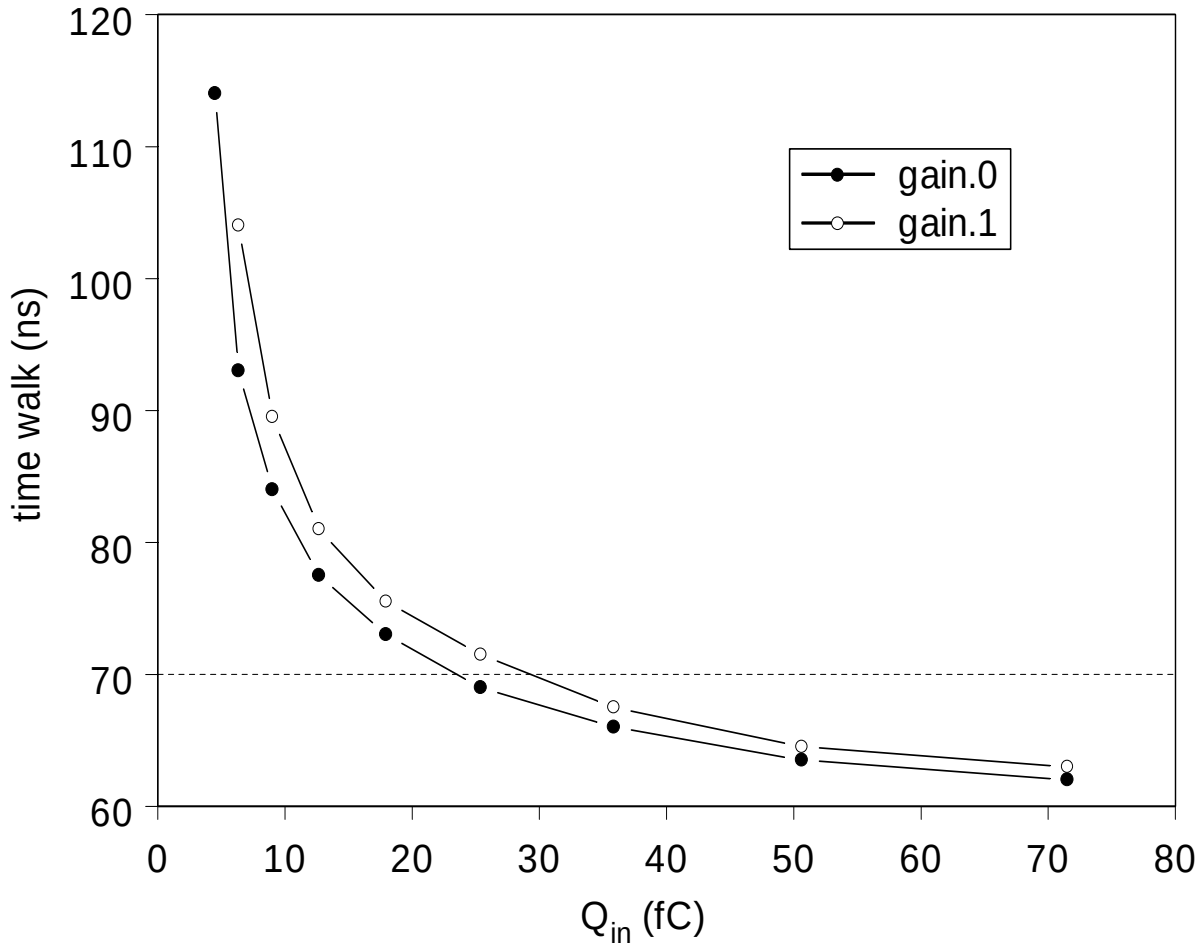

Figure 8: Time walk (ns) versus input charge (fC) for the two different gain stettings.

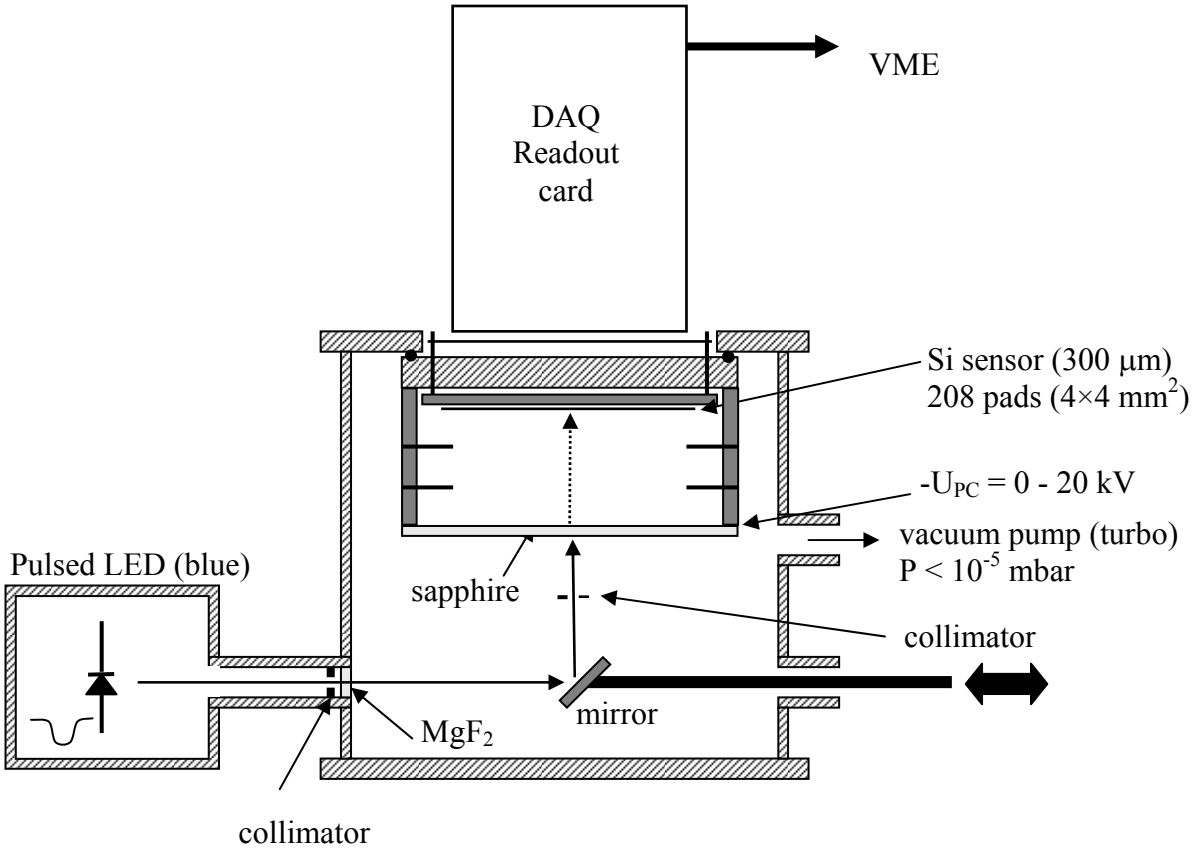

Figure 9: Set-up to test the PET-HPD with a pulsed LED.

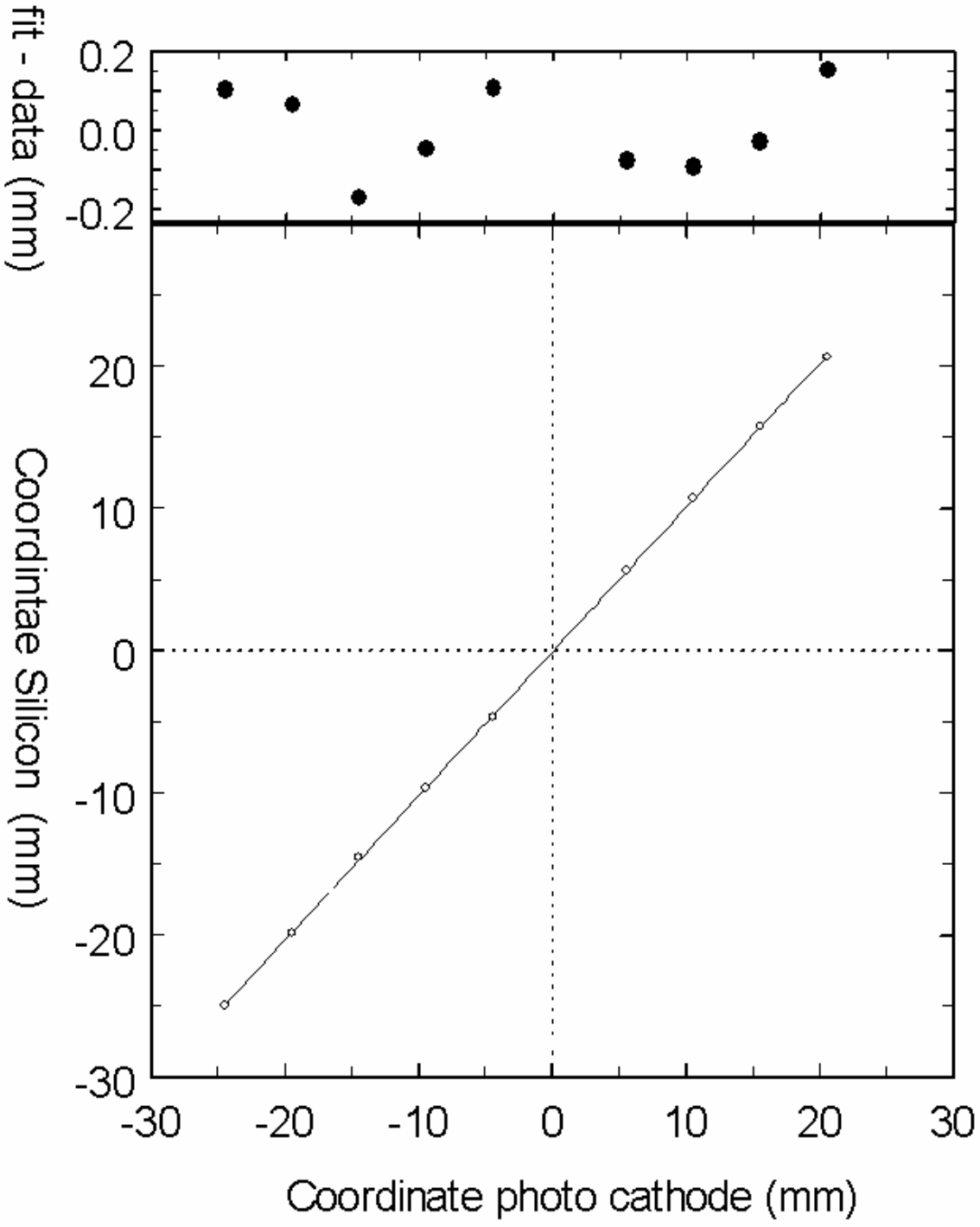

Figure 10: Mapping between photocathode and Silicon sensor. The relation is purely linear, deviations are of the order of 60 μm (RMS).

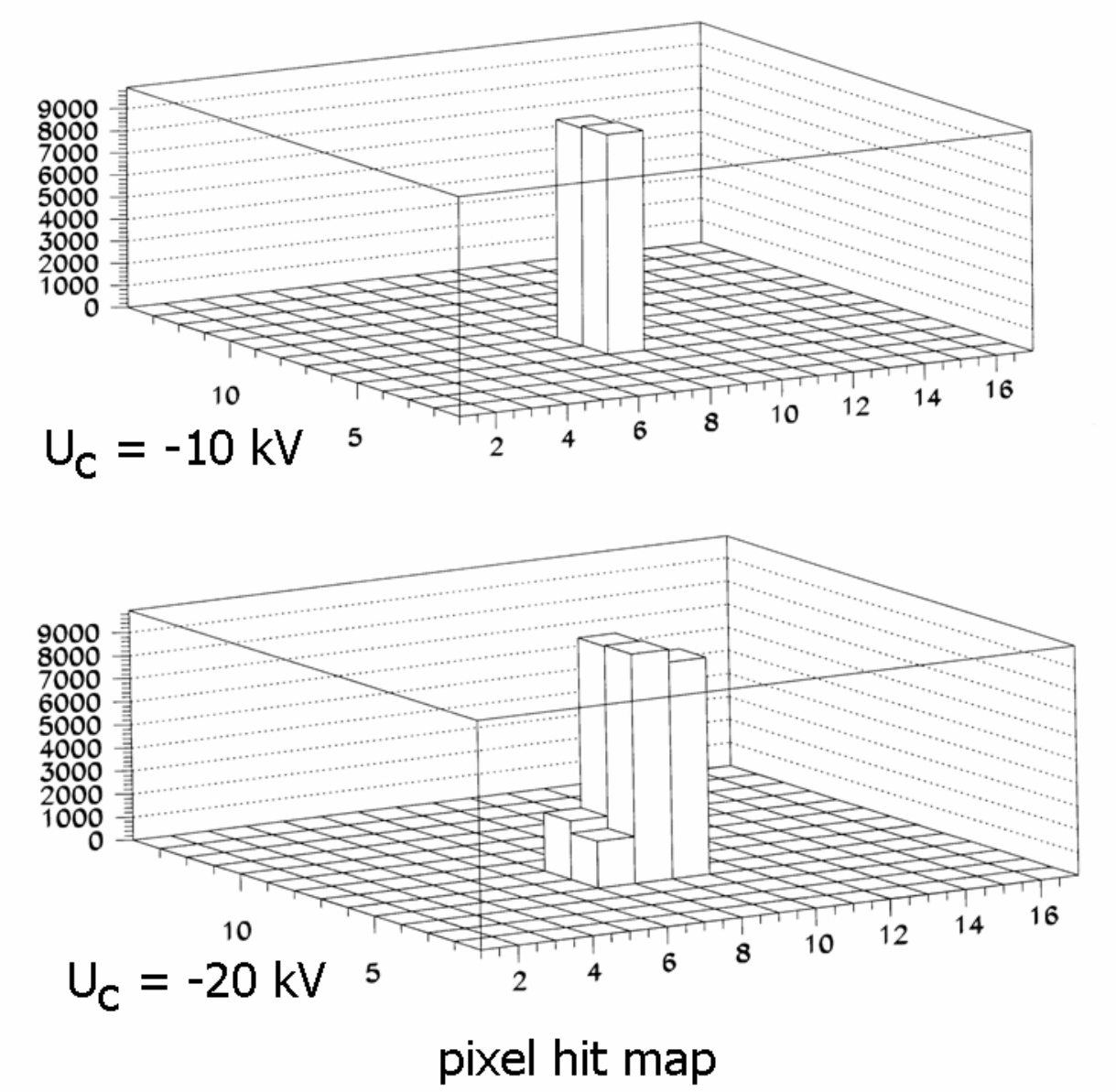

Figure 11: PET-HPD hit maps at U_C = -10 and -20 kV.

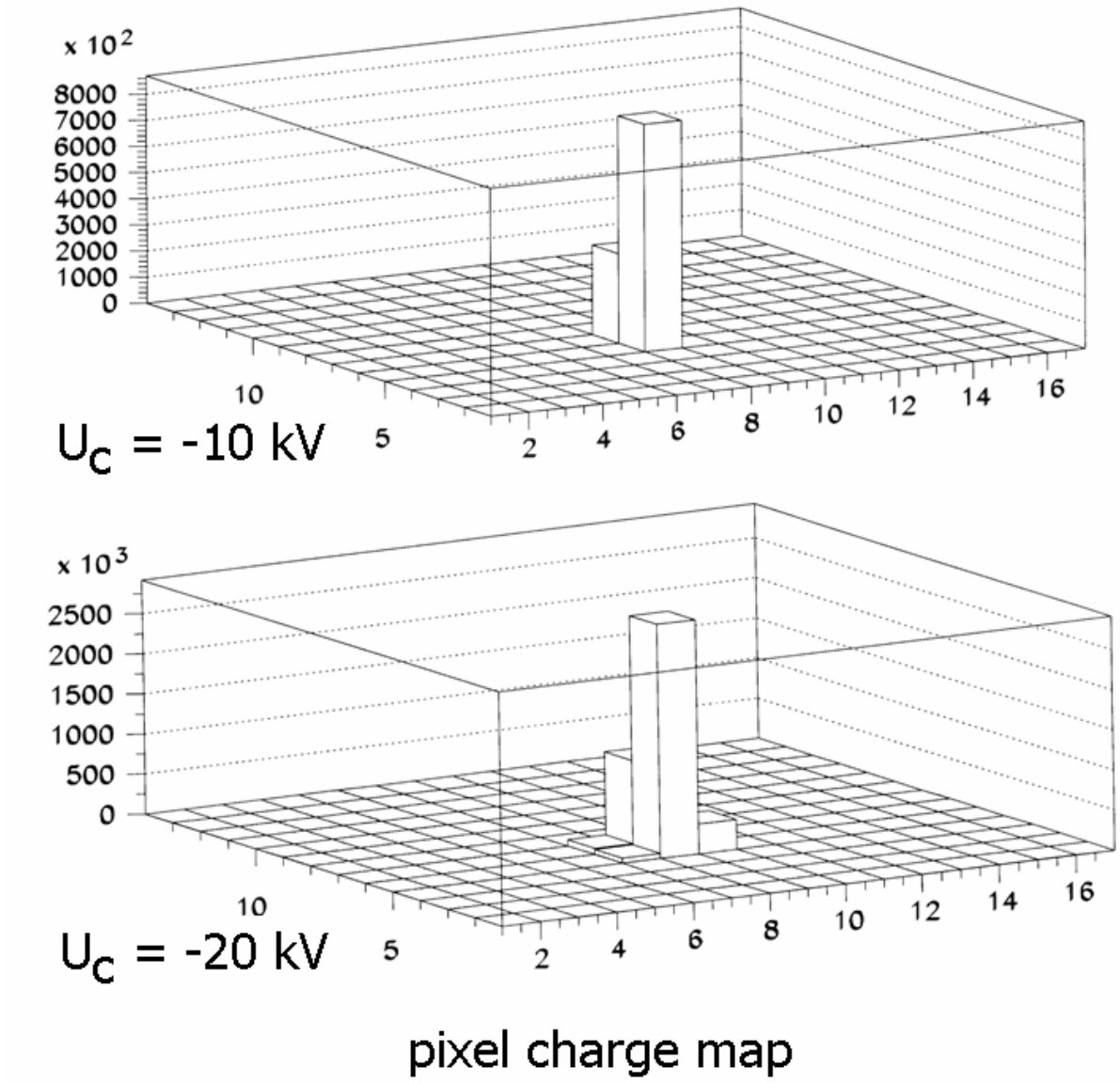

Figure 12: PET-HPD charge maps at U_C = -10 and -20 kV.

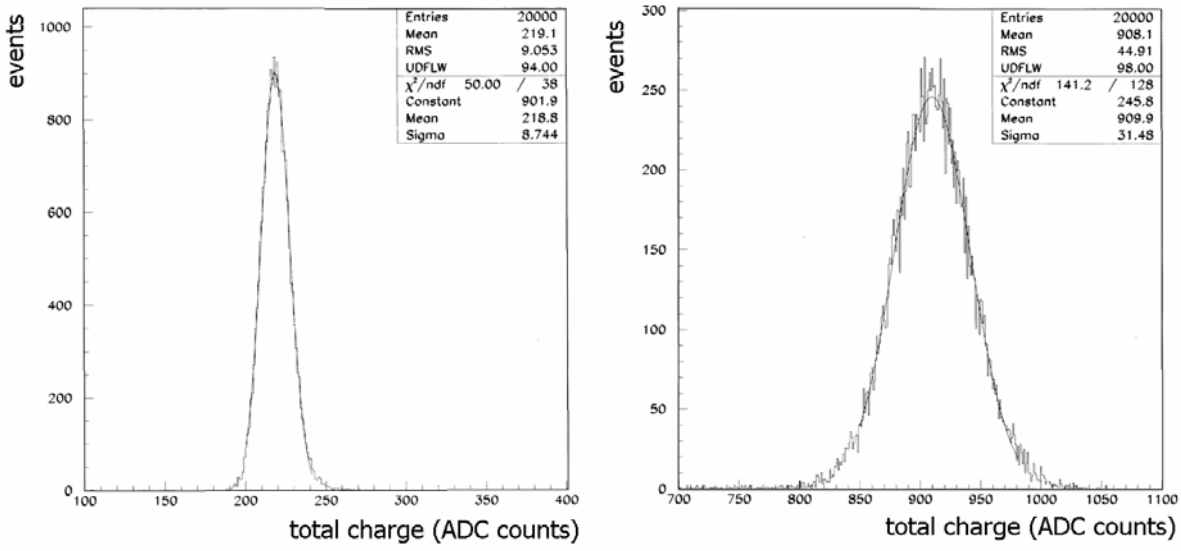

Figure 13: Histograms of the total charge for two different HPD acceleration voltages. Left: U_C = -10 kV ; Right: U_C = -20 kV.

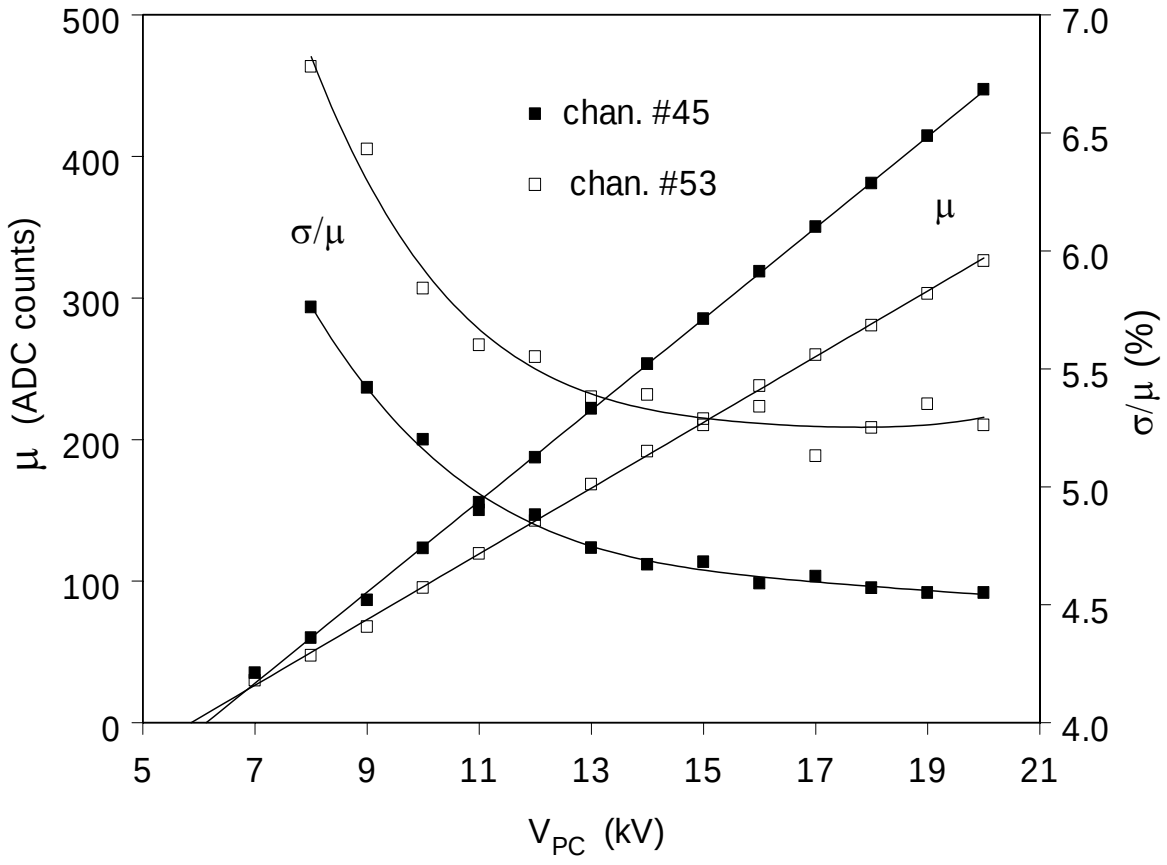

Figure 14: Mean charge μ (left axis) and ratio of Gaussian width to mean charge σ/μ (right axis) versus cathode voltage U_C (kV).

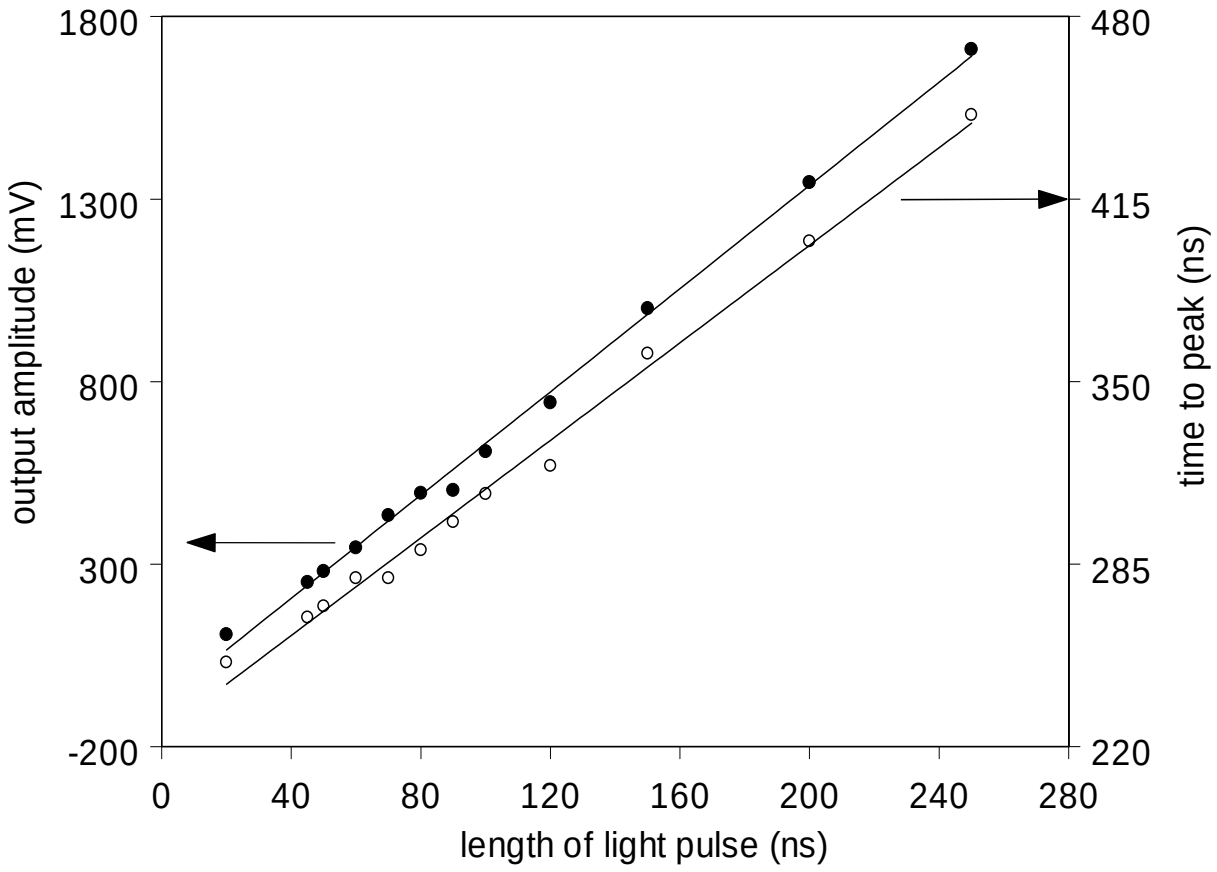

Figure 15: Analogue output amplitude (full symbols, left scale) and time to peak (empty symbols, right scale) versus the length of the LED pulse.

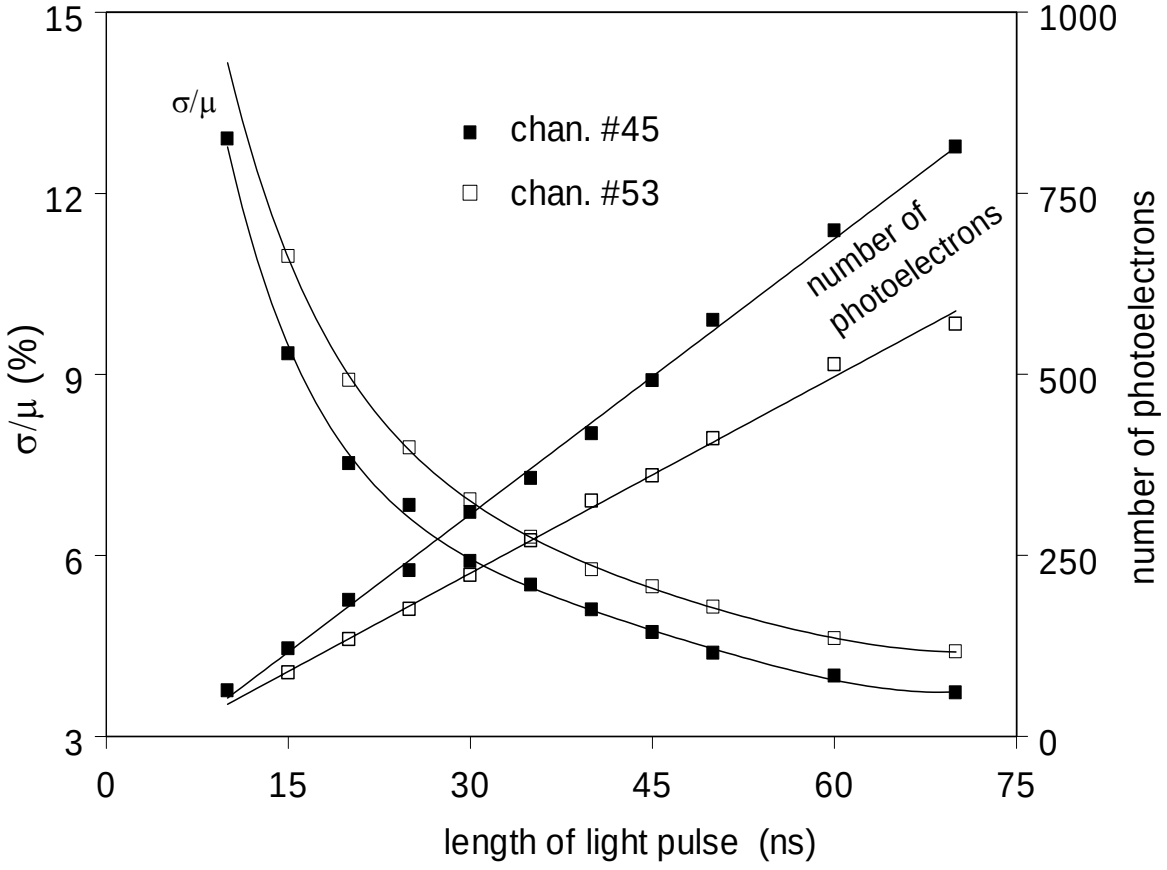

Figure 16: The variation of the relative energy resolution (left scale) and the derived number of photoelectrons (right scale) are plotted versus the length of the LED light pulse.